Large Eddy Simulation of turbulent hydrogen-fuelled supersonic combustion in an air cross-flow

The main aim of this article is to provide a theoretical understanding of the physics of supersonic mixing and combustion. Research in advanced air-breathing propulsion systems able to push vehicles well beyond Ma = 4 is of interest worldwide. In a scramjet, the air stream flow captured by the inlet is decelerated but still maintains supersonic conditions. As the residence time is very short (<1ms), the study of an efficient mixing and combustion is a key issue in the ongoing research on compressible flows. Due to experimental difficulties in measuring complex high-speed unsteady flow fields, the most convenient way to understand unsteady features of supersonic mixing and combustion is to use computational fluid dynamics. This work investigates supersonic combustion physics in the Hyshot II combustion chamber within the Large Eddy Simulation framework. The resolution of this turbulent compressible reacting flow requires: (1) highly accurate non-dissipative numerical schemes to properly simulate strong gradients near shock waves and turbulent structures away from these discontinuities; (2) proper modelling of the small subgrid scales for supersonic combustion, including effects from compressibility on mixing and combustion; (3) highly detailed kinetic mechanisms (the Warnatz scheme including 9 species and 38 reactions is adopted) accounting for the formation and recombination of radicals to properly predict flame anchoring. The simulation was performed by means of the ENEA homemade code HeaRT and it was runned on the CRESCO platform. Numerical results reveal the complex topology of the flow under investigation. The importance of baroclinic and dilatational effects on mixing and flame anchoring is evidenced. Moreover, their effects on turbulence-scale generation and the scaling law are analysed

■ D. Cecere, E. Giacomazzi, F.R. Picchia, N.M. Arcidiacono

Introduction

The importance of mastering hypersonics lies in applying it to space launchers and trans-atmospheric commercial vehicles. This renewed interest in high-speed flight requires significant developments, particularly, in the field of propulsion. Vehicles capable of such speeds are being tested now in the US (HyTech, HyV), Russia and the UK–Australia (HyShot), Japan, India, China, and Korea. EU is funding the project LAPCAT to study the feasibility of a long-range hypersonic commercial transport.

Propulsion systems using external air, like ramjets and supersonic combustion ramjets, can save a large fraction of the weight (and bulk) of carrying on-board liquid oxygen (LOx). Ramjet engines, in which the incoming airflow speed is decreased to subsonic speed, can be efficiently used for Ma = 3−5 flight regimes; but

Contact person: Donato Cecere
donato.cecere@enea.it

beyond these speeds, alternative propulsion systems are required. The supersonic combustion ramjet (or scramjet) engine, where the incoming airflow is decelerated but remains supersonic, is one of the most promising propulsion options. An air-breathing launcher, using external air captured by a hypersonic engine, such as a scramjet for its first stage, may reduce orbiting costs by about one order of magnitude [1, 2].

The main problem of supersonic combustion is that the residence time at supersonic speed is very short. Hence, mixing enhancement and combustion efficiency are two key issues to be investigated. In fact, no theoretical (physical) understanding ever came out.

The study of mixing and combustion in supersonic flows is the topic of an on-going research, rich in problems involving theory and modelling and having fundamental and applied significance. In fact, when a gaseous fuel jet is injected into a supersonic crossflow, the fuel acts as an obstruction to the crossflow and produces a strong shock wave. This shock interacts with the boundary layer on the wall to form a complex flow system, in which supersonic and subsonic pressure regions coexist near the injector.

The purpose of this paper is to obtain additional insights into the 3D unsteady flow processes of the su-

personic jet mixing by numerically simulating the Hyshot II test case. For this purpose, a highly accurate non-dissipative numerical scheme to properly simulate the strong gradients near the shock waves and the turbulent structures away from these discontinuities has been developed by the authors.

The HyShot II scramjet test case

The HyShot Flight Program is an experiment designed to develop a correlation between pressure measurements of supersonic combustion in The University of Queensland's T4 shock tunnel, and that observed in flight experiments. In the flight tests, the Hyshot scramjet was accelerated up to Mach 8 using a Terrier-Orion sounding rocket. The sounding rocket reached a maximum altitude of 330 km. Before re-entry the sounding rocket and scramjet were maneuvered into the experimental altitude. Between the altitudes of 23 and 35 km, gaseous hydrogen was injected into the scramjet and pressure sampled. A flight Mach No. of 7.6 with a 3-sigma variation of 0.2 was registered. The ground-based tests were performed in the T4 shock tunnel at the University of Queensland [3] and in the High Enthalpy Shock Tunnel Göttingen (HEG) of the German
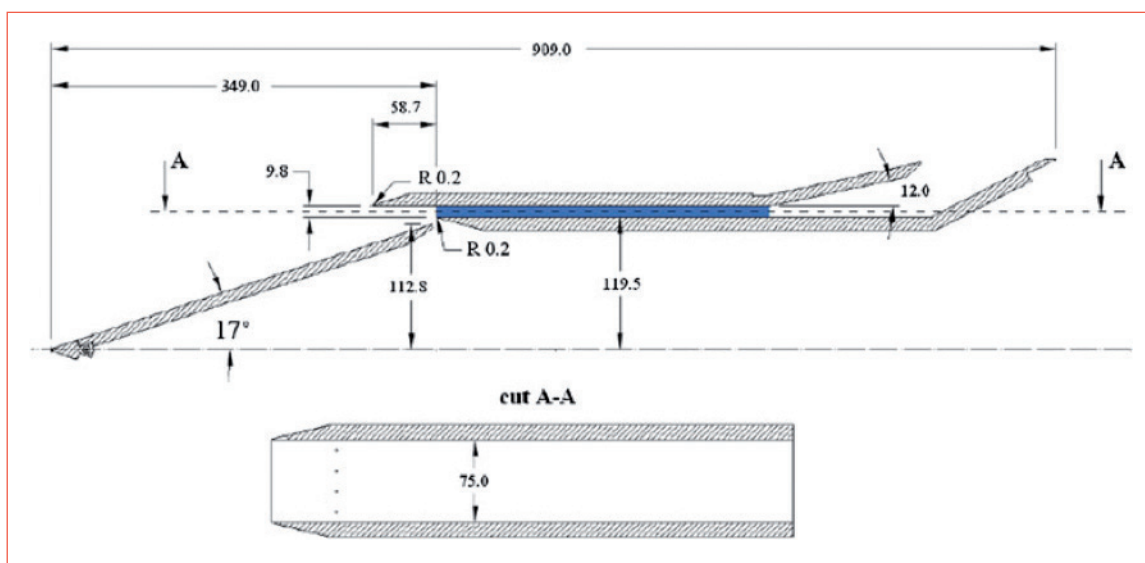

FIGURE 1 Hyshot schematic; portion of the combustion chamber simulated in blue

Aerospace Centre (DLR) [4, 6], at different conditions so as to obtain correlations with flight-based tests.

The HyShot scramjet geometry used in the ground experiments features a rectangular air intake 305-mm long and 100-mm wide, a combustor 300-mm long and 75-mm wide and 98-mm high, a thrust plate 200-mm long x 75-mm wide. The intake is a 17° inclined wedge compressing the incoming hypersonic flow (Figure 1). The combustor hosts 16 pressure transducers starting from 90 mm downstream of the combustor leading edge. Distance between nearby pressure transducers is 13 mm. The thrust plate is at 12° with respect to the airstream path and is equipped with 11 pressure transducers, located 11 mm downstream of the combustor exit. The gaseous hydrogen is injected in crossflow with respect to the incoming air by means of four 2-mm portholes injectors, located 40 mm downstream of the leading edge of the combustor inner surface. In this work, the design condition defined as 0° angle of attack, nominal altitude of 28 km and flight Mach number of $Ma = 7.6$ has been selected for numerical simulations. The associated scramjet inlet conditions are those reported in Table 1 [3]. The global equivalence ratio is 0.426. The only available ground experimental data at these conditions are pressure history and wall distribution from the University of Queensland [3]. Wall pressure, heat transfer, and OH distribution from DLR are instead available at different equivalence ratios and angles of attack not analysed in the present study [6]; therefore, only qualitative comparisons are provided with those results. However, in [3], the effect of the angle of attack on the pressure history has been studied, whereas in [4], the effect of the equivalence ratio is analysed.

	Air inlet	Fuel inlet
Pressure (Pa)	82,210	307,340
Mach no.	2.79	1
Density (kg/m³)	0.2358	0.3020
Temperature (K)	1,229	250
Sound speed (m/s)	682.9	1201.4
Flow velocity (m/s)	1905.291	1204.4

TABLE 1 Combustor inlet flow conditions for the test at 0° angle of attack analysed in this work

Numerical simulation

In the present study, the blue portion of the combustion chamber sketched in Figure 1 is simulated using the inlet flow conditions reported in Table 1. To properly simulate the flow velocity at the combustor entrance, a realistic velocity profile has been imposed at the combustor inlet as the well developed boundary layer must be taken into account. This profile has been obtained numerically by Jeung et al. [7], and also includes the effect of the intake. In the present simulation, no synthetic turbulence was generated at the inlet. The vortical structures predicted develop naturally due to the strong turbulence forcing in the flow field, e.g. the bow shock and the strong gradients at walls. At the inlet, all quantities are prescribed, except density in the subsonic regions, by means of characteristics inflow boundary conditions. Partially non-reflecting boundary conditions have been implemented (following the NSCBC technique [8, 9]) to reduce the numerical reflection of acoustic waves back into the computational domain, where subsonic regions are present. Because of the short-testing time, all walls are assumed to be adiabatic. In fact, since the Large Eddy Simulation (LES) is necessarily much shorter than the flight time, it is likely to have no large differences in the results obtained using a fixed wall temperature boundary condition, or a nil heat diffusive flux. Actually, for a fixed wall boundary condition the heat diffusion characteristic time (about 10^{-2} s) is longer than the characteristic convective time (about 10^{-4} s) of the flow.

In the present LES simulation, the fuel hole geometry is treated by means of an immersed boundary technique [10, 11].

Transport equations

In LES, each turbulent field variable is decomposed into a resolved and a subgrid-scale part. In this work, the spatial filtering operation is implicitly defined by the local grid cell size. Variables per unit volume are treated using the Reynolds decomposition; the Favre, density weighted, decomposition is used to describe quantities per mass unit. The instantaneous small-scale fluctuations are removed by the filter, but their statistical effects remain inside the unclosed terms representing the influence of the subgrid scales on the resol-

ved ones. Gaseous combustion is governed by a set of transport equations expressing the conservation of mass, momentum and energy, and by a thermodynamic equation of state describing the gas behaviour.

The spatially filtered Navier–Stokes equations are solved by means of a finite difference method on a Cartesian non-uniform grid in a collocated cell-centred variable arrangement, together with an explicit, fully compressible solver. In writing the numerical scheme, the focus was on the numerical approximation of the derivatives in the advection terms at the resolved scales. Due to the high gradients in the flow, fluxes are evaluated by a hybrid method capable of capturing shocks without introducing numerical unphysical oscillations in regions where high gradients are present and, at the same time, capable of resolving with low-dissipation turbulent structures away from discontinuities.

Convective fluxes have been calculated by means of a shock capturing or a low-dissipation scheme, accordingly to a sensor based on the density and pressure fields [22].

In the shock capturing scheme, the reconstruction of the Riemann problem (necessary in a compressible flow to correctly evaluate gasdynamic properties evolution) at the cell interface is performed by means of a Weighted Essentially Non Oscillatory (WENO) of order 3–5 scheme The interface fluxes from the reconstructed states have been obtained by implementing the approximate hybrid HLLC/HLLE Riemann solver [25]. In the region, where the flow is smooth, the convective derivatives are determined by means of a fourth-order central finite difference scheme [26]. Time integration is performed by means of the fully explicit third-order accurate TVD Runge-Kutta scheme of Shu and Osher [27]. For numerical stability the time-step was about 10^{-9} s. The N.- S. equations are thus fully coupled. The simulation was performed by means of the ENEA homemade code HeaRT and it was run on the CRESCO platform.

Numerical results

The results of the 3D LES of the HyShot II combustor with a grid of 52M cells are now shown. The computational grid is more refined close to and within the flow injectors, and stretched in the second half of the combustor. A grid sensitivity analysis was performed in [29]. In that paper, three different grids were adopted: a coarse grid of 14M cells, a grid of 52M cells and a refined grid of 71M cells (these grids were refined close to and within the flow injectors, and stretched in the se-
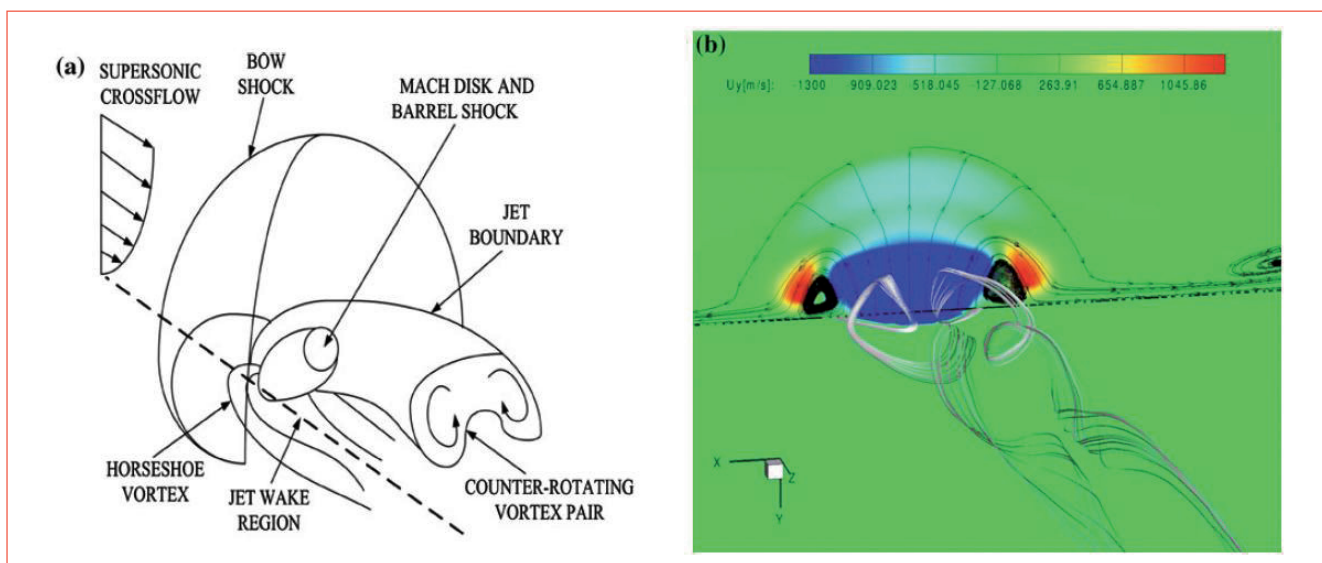

FIGURE 2 Schematic of transverse injection into a supersonic flow [32] **(a)**. Side views near a hydrogen injection hole of the HyShot II scramjet engine, showing a slice of U_y velocity field at x = 0.0281 m and a counter-rotating vortex pair **(b)**

cond part of the combustor). Differences between the intermediate and the refined grid were negligible; in particular, comparison showed that the larger turbulence structures and the shock waves were well predicted for both the two different grids. The recirculation region located upstream and downstream of the jet injection was well identified for both grids, but it was much more spread for the refined grid; the hydrogen jet was also less identifiable at the end of the combustor and the flame diffusion was higher. In fact, a critical role in the fuel/air mixing is given by the small vortex structures arising from the boundary layer and providing the convection of H_2 within the upstream and downstream recirculation region, between the injectors, at the air/fuel interface and downstream of the shock waves. For these three grids, going from the more refined to the coarser grid, $u*y/\nu$ (where u is the velocity, y the distance from the wall, and ν is the kinematic viscosity) goes y^+ from ~2.5 to 4 and 15. In [28], it was observed

that mainly streamwise streak structures arise in the range of y^+ = 5 to 40~50. Hence, y^+ ~4 adopted in the present simulation guarantees the streaks formation at the wall, their evolution within the turbulent boundary layer and the outer flow, and the shock boundary layer interaction.

As a preliminary conclusion by [29], it was stated that when the focus is on the physical understanding of mixing and combustion in supersonic flows and on the vorticity generation and transport it is important to have a rather refined grid, when the focus is posed on the flame-anchoring prediction or combustion efficiency calculation, also a coarser grid (y^+ not higher than 5), but always able to capture the 3D shock structures, the shock boundary layer interaction and the large-scale turbulent structures are enough. The numerical results of the HyShot II scramjet engine (see [30] for other details) show that the hydrogen jets expand rapidly, obstructing the supersonic crossflow and producing a 3D bow shock ahead of each injector, as shown in Figure 2. In Figure 3a, clearly identified are the formation of shock waves at the upper wall combustor entrance, the generation of a train of shock waves reflecting from the bottom wall and impinging the flame front, the formation of the 3D bow shock due to the H_2 crossflow injection within the airstream, the barrel shock, and Mach disk (see also Figure 3b).

Figure 3 shows that the bow shock is located about 1 mm ahead of the transverse fuel injection: here the temperature increases, reaching about 2,200 K. Once hydrogen is injected within the airflow, it expands rapidly reaching its lower temperatures (T = 150 K) before barrel-shock recompression. The pressure increase due to this recompression is responsible for the boundary layer thickening and separation (located 20 mm upstream of the injectors, see Figures 3a–c, 5) and a consequent formation of the hairpin shocks (see Figure 4); here, two spanwise vortices are trapped within, approximately, the subsonic recirculation region between the upper wall and the shocks. Hydrogen penetrates the airflow of 2.5D at a streamwise distance of 7D from the center of the injection hole. The bow shock strength varies with respect to the distance measured from the injector wall. Away from the wall, the bow shock curves around the injectant plume. Due to the expansion of the
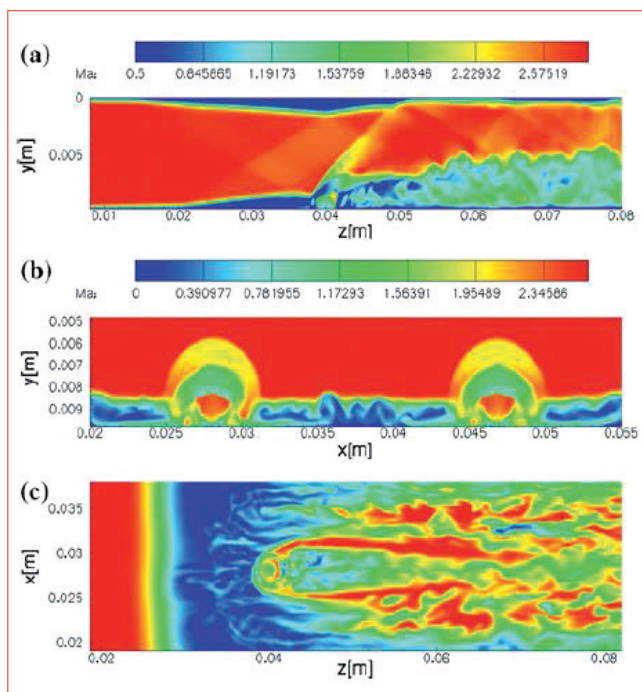
FIGURE 3 Instantaneous snapshots of the Mach number in the HyShot II scramjet engine: midline plane x /d = 14.15 **(a)**, transverse plane z/ D = 30 **(b)**, and wall-parallel plane y/ D = 0.5 **(c)**

injected jet and its interaction with the bow shock, complex shock waves are generated in the injectant plume, including a barrel shock and a Mach disk. Furthermore, the adverse pressure gradient close to hydrogen injection causes the separation of the upstream wall boundary layer, also revealed in the experimental tests above an equivalence ratio of 0.474 [6, 31]. Hence, a subsonic region is formed (see Figure 3) where hydrogen and air mix quickly (see Figure 4) and consequently the fla-

me holds, as evidenced by OH and H_2O concentrations, and temperature distributions in Figures 4, 5, 6 and 7, in qualitative agreement with the experimental excited OH* radicals reported in Figures 8 and 9.

Note that the experimental visualization of OH*, OH*-excited radicals, captured by means of chemiluminescence, is at a lower equivalence ratio and higher angle of attack than those numerically simulated. Actually, the numerical OH prediction is qualitatively closer to the numerical results predicted in [6], where the presence of OH, both in front of the injection point and in the shear layer immediately downstream of the injectors, was predicted. In fact, as already explained by Laurence at al., numerical results show levels of the OH molecule, rather than the OH-excited radical. However, the axial location of the onset of the main combustion region and the penetration of the flame into the combustion chamber further downstream show reasonable agreement. Furthermore, qualitative comparisons between numerical and experimental OH predictions show a good agreement, predicting high-OH presence at the combustor exit.
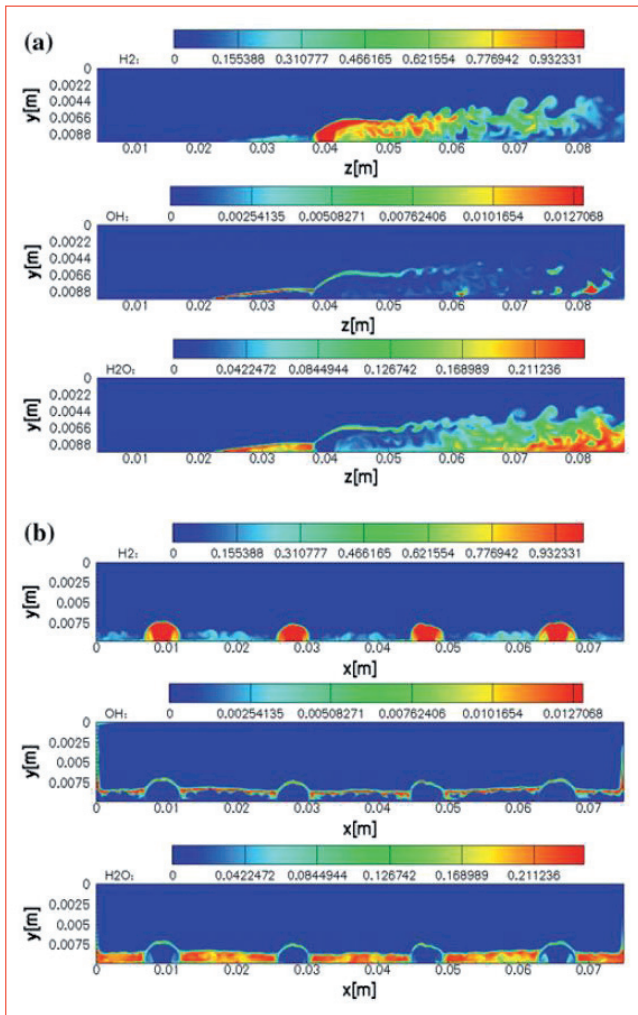

FIGURE 4 Instantaneous mass fraction fields for H_2, H_2O, OH at the plane x = 2.81 cm **(a)**, and instantaneous mass fraction fields for H_2, H_2O, OH at the plane z = 4.0 cm **(b)** in the HyShot II scramjet engine
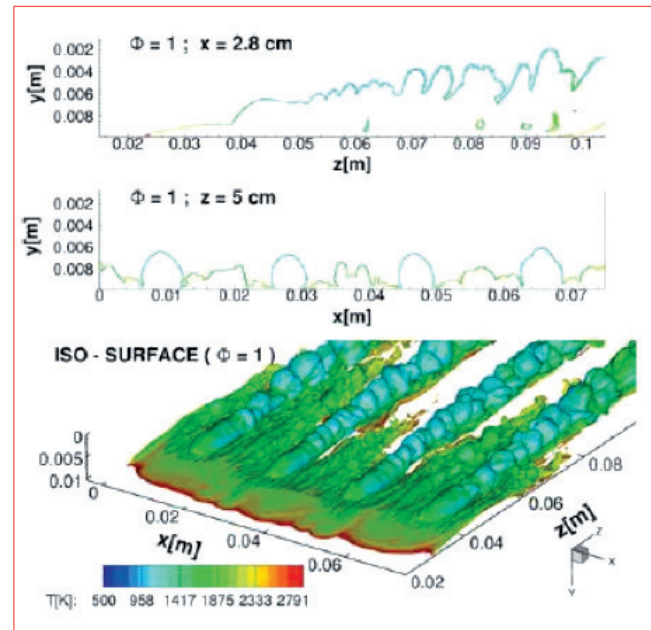

FIGURE 5 Instantaneous stoichiometric flame surface coloured by temperature, and section views of numerical results of the HyShot II scramjet
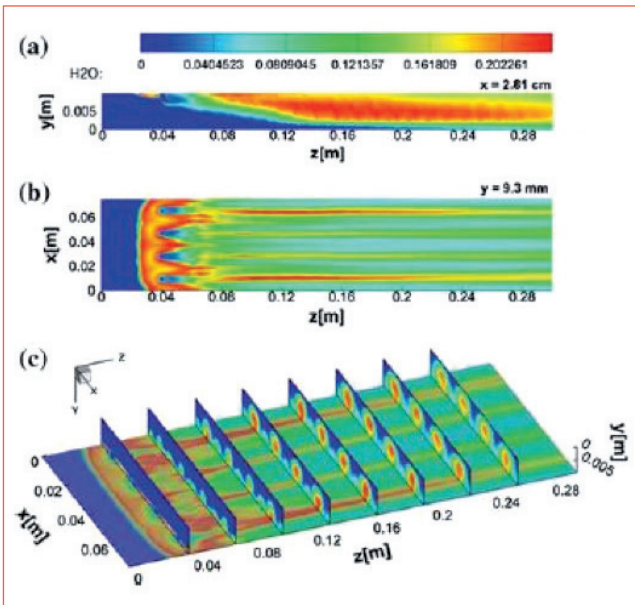
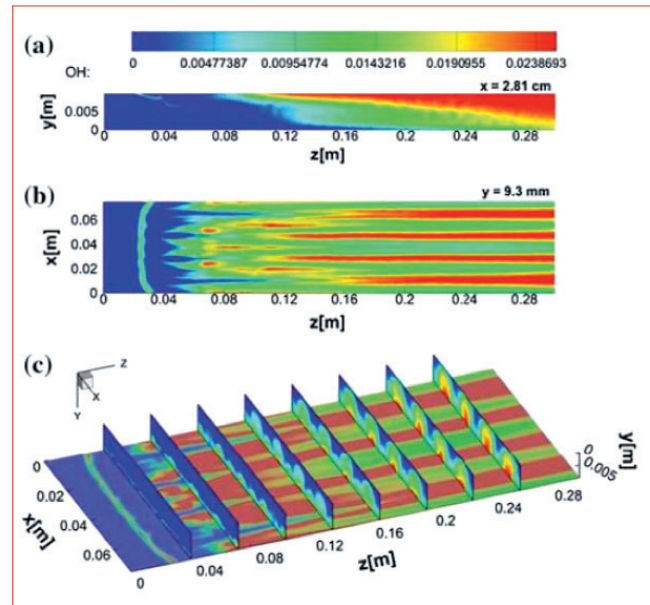FIGURE 6 Averaged H_2O mass fraction in the HyShot II scramjet engine

FIGURE 7 Averaged OH mass fraction: midline plane x /d = 14.15 **(a)**, transverse plane z/ D = 30 **(b)**, and wall-parallel plane y/ D = 0.5 **(c)**

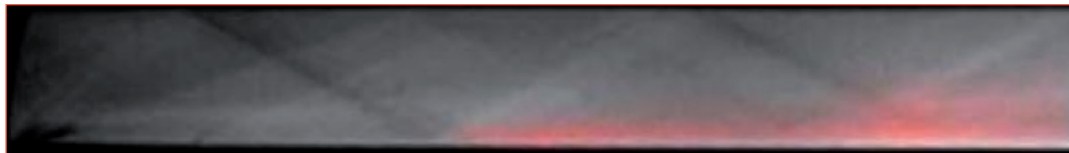FIGURE 8 Experimental composite OH* visualization for an equivalence ratio of 0.35

FIGURE 9 Composite experimental Schlieren image with composite OH* levels superimposed (red) near the hydrogen injection point (lower left) for an equivalence ratio of 0.35

Numerical simulations show that in the recirculation zone mixing is mainly driven by spanwise vortices, whereas in the jet shear layer it is driven by streamwise structures that increase the interfacial fuel/air area and convect hydrogen from the jet core outwards. Due to the blockage of the supersonic cross flow by the fuel injection (the momentum depending also on the equivalence ratio), a horseshoe vortex tube is formed near the wall. In the injectant plume, a pair of counter-rota-

ting vortex tubes are also developed. The streamwise counter-rotating vortex pair contributes to engulf the air freestream, and the horseshoe vortex wraps around the hydrogen jet and flows downstream along the wall transporting hydrogen there, as shown in Figure 4.

Close to the combustor exit, the flame occupies the whole combustor section. There, a high OH concentration (about 25%) is observed, due to the H_2O dissociation produced by the high temperatures. In about 15

orifice diameters (3 cm downstream of hydrogen injection) the fuel fraction is reduced by 50%. The combustion efficiency at the outlet of the combustion chamber

$$\eta^c = 1 - \left(\int_A \overline{\rho} \, |\tilde{u}| \, Y_{H2} \, dA \right) / (\overline{\rho} \, |\tilde{u}| \, Y_{H2})_{inlet}$$

ρ density
Y_{H2} *mass fraction of H_2*
u *velocity*

is found to be about 87.65%.

Figure 10a compares the numerical and the HyShot-T4 Supersonic Combustion (Queensland) experimental pressure distribution along the upper wall ($Y = 0.0098$ m) of the combustion chamber at $X = 3.5$ cm and 1.32 ms. The trend is well predicted in the first part of the combustor, where the grid is much more refined. Better agreement near the exit region needs a finer grid to capture shock reflection.

A good agreement was also obtained in Figure 10b, comparing numerical and HyShot-T4 Supersonic Combustion (Queensland) experimental pressure time evolution at a point on the upper wall ($Y = 0.0098$ m and $Z = 0.272$ m). Actually, these numerical results show a better trend agreement with the High Enthalpy Shock Tunnel Göttingen (HEG) experimental results, where the pressure jumps are less sharp with respect to the HyShot-T4 Supersonic Combustion Experiments (Queensland). Unfortunately, only conditions at a non 0° angle of attack have been performed in the HEG, thus no quantitative comparisons with these data are feasible [4].

Mixing in supersonic flows

Theoretical results in [33] showed that in supersonic flows the compressibility, vortex stretching and baroclinic terms of vorticity equation are all of the same order of magnitude. Experimental and numerical results, respectively in [34] and [30], confirmed these expectations and showed that these terms can contribute to air/fuel mixing and combustion in an equal way but in different regions. Moreover, experimental observations proved that streamwise vorticity, easily found in supersonic combustion, enhances mixing at the molecular level and leads to short flames and efficient combustion [34-39]. Figure 11 shows that the vorticity is approximately zero about the exit of the hydrogen injector. Then, it becomes extremely high (~10^6 Hz) immediately af-
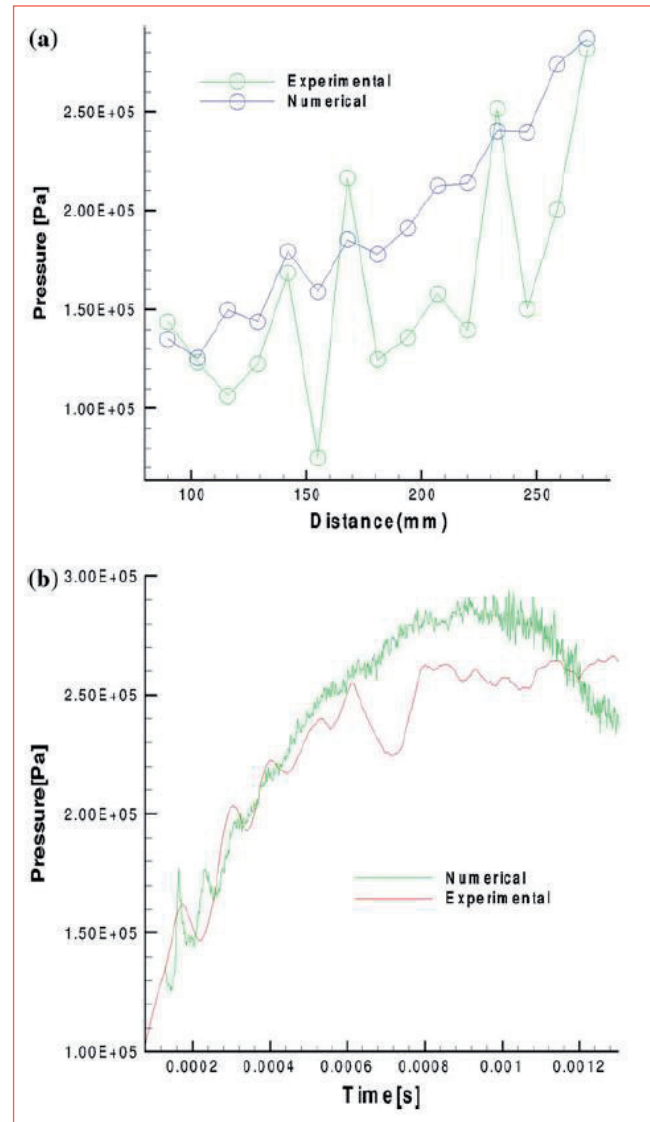

FIGURE 10 Comparison of numerical and HyShot-T4 Supersonic Combustion (Queensland) experimental pressure distribution along the upper wall at X = 3.5 cm **(a)**. Comparison of numerical and HyShot-T4 Supersonic Combustion (Queensland) experimental time evolution at a point on the upper wall (Y = 0.98 cm and Z = 27.2 cm) **(b)**

ter it penetrates the airflow core, where, accordingly, mixing times should be ~10^{-6} s. In the region upstream of the fuel injection, the vorticity magnitude is ~10^7 Hz. Here, the larger contribution to vorticity is given by the spanwise and crosswise vorticity components. Down-
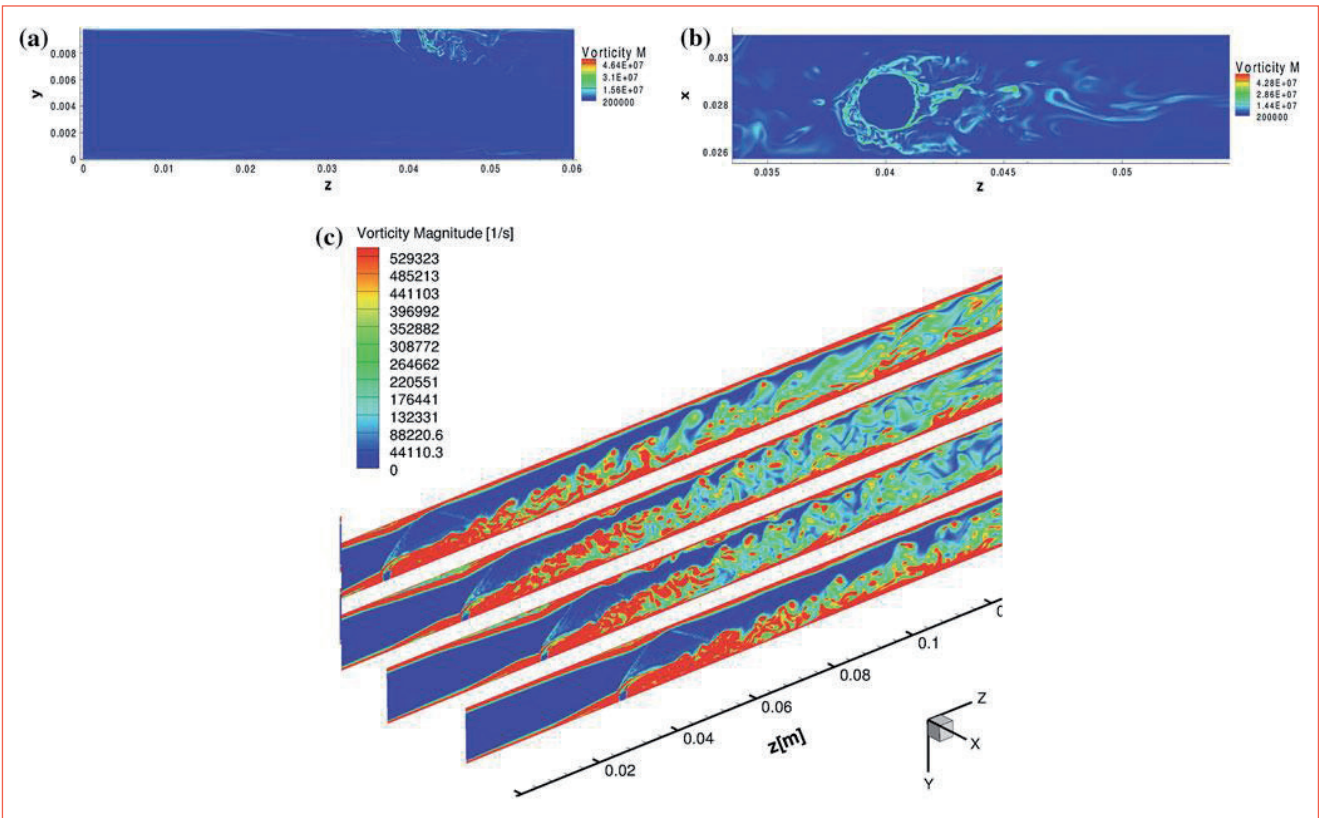
FIGURE 11 Instantaneous flowfields of vorticity magnitude in the HyShot II scramjet engine at x/d = 14.15 **(a)** and at the wall-parallel plane y/d = 1 **(b)**. Flowfields of vorticity magnitude at constant X planes are in **c**, with a range scale smaller than in a and b to cut out peaks in the H_2 injection region

stream, due to the interaction between ω_x (vorticity) and the transverse velocity gradients, vortex stretching tilts vorticity in the streamwise direction, resulting in the formation of horseshoe vortices (see Figure 2).

The baroclinic effect (due to the coupling of density and pressure gradients and generally negligible in subsonic non-reacting flows) is particularly effective in producing the rapid mixing and the consequent anchoring in the present supersonic test case (see Figure 12). In fact, shock waves generate high density and pressure gradients. The highest peak of the baroclinic term, of the order of 10^{12} s^{-2}, is located where the hydrogen jet rapidly expands and strong shock structures are present. Here, the coupled effect of high density and pressure gradients is enhanced by the low hydrogen density (ρ~0.03kg/m^3).

Physically speaking, the baroclinic term supplies the rate at which the vorticity is generated and pumped into the flow. In practice, this means that if there were no dissipative phenomena and if the baroclinic-driven spin acceleration was constant, e.g., 10^{12} s^{-2}, the spin speed, i.e., the vorticity, would increase by 10^9 Hz each ms.

This is in essence the baroclinic mechanism enhancing mixing in supersonic combustion. It is per se a key observation for applications, because it underlines the importance of the combustor geometry and injector configurations. Indeed, in that presented here, the pressure and density gradients are due to "shocks" triggered by the crossflow H_2 injection. However, the strong source of vorticity notwithstanding, this injector configuration may result in significant total pressure losses and lower thrust. Other injector configurations with the
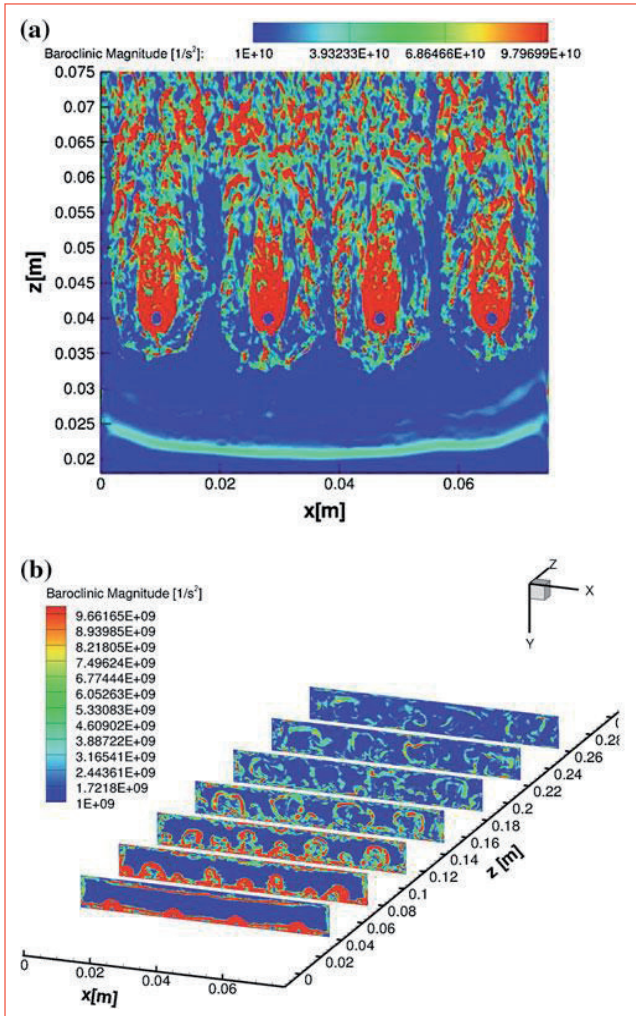
FIGURE 12 Baroclinic term magnitude in the HyShot II scramjet engine: slices on the four middle-plane inlet orifices **(a)**, slices at different z planes from z/d = 20 to z/d = 130 **(b)**

same capability to produce vorticity, but with (presumably) lower total pressure loss, should be investigated.

Effects of compressibility on turbulent scaling and scales
In supersonic flows, far from shocks and walls, the vorticity and the velocity vectors are expected to be nearly aligned [34], i.e., turbulent structures are mainly streamwise. This implies that in those regions the helicity $H = \omega \cdot \boldsymbol{u}$ (where omega is the vorticity and u the velocity vector) nearly peaks. The helicity gives a reasonable idea of the rotational acceleration of the flow. When

helicity locally peaks, the term of vorticity transport equation responsible for the turbulent kinetic energy cascade in subsonic flows, composed by the convective transport and the vortex stretching terms, i.e., $\nabla \times (\omega \times \boldsymbol{u}) = (\boldsymbol{u} \cdot \nabla) \omega - \omega \cdot \nabla \boldsymbol{u}$, reaches a minimum. Thus, where helicity locally peaks, the classic contributions to the turbulent kinetic energy cascade in subsonic flows are negligible and the baroclinic and dilatational terms of the vorticity transport equation could be responsible for a turbulent energy decay different from the well-known −5/3 Kolmogorov scaling [33].

In [33], a slope steeper than Kolmogorov's −5/3 was theoretically found. In particular, by means of the Buckingham– Riabucinski (π) theorem applied to the turbulent kinetic energy per unit mass and wave number with functional dependencies on the wave number k, the dissipation rate per unit volume $\rho\varepsilon$, and the mass M, it was observed that $E \sim C k^{-11/3} (\rho\varepsilon)^{2/3} M^{-2/3}$. DNS simulations [40] also revealed a k^{-4} decay in the kinetic energy spectrum, and experiments in [41] showed a $k^{-11/3}$ decay in the core of flows at Mach 6 up to 7.5.

To verify the slope deviation from that predicted by the Kolmogorov theory, energy spectra at different "probed" points of the HyShot II supersonic combustion chamber have been derived. The sampling time is 1.3 ms (with 1,955 samples), so the resolution in frequency (~770 Hz) is coarse at large scales. Hence, low frequencies in Figure 13 are not shown. The sampling frequency is about 1.5 MHz: according to the Nyquist–Shannon sampling theorem, the maximum frequency that can be observed is thus 750 kHz.

The first probe (m1) is located upstream of the injectors at about half height ($y = 4.5$ mm); the second one (m2) is located at the same height but a little further downstream of the bow shock.

The other two (m3 and m9) are located in the middle of the combustor close to the wall (injection side) at $z = 9$ cm and $z = 16.8$ cm, respectively: they are inside the central vortex core and subjected to alternating compression and expansion cycles due to the interaction of the shocks formed by the two central injection jets.

At all points, the spectra show an inertial decay with a slope close to −11/3 for frequencies higher than 10^5 Hz, and a tendency for a −5/3 scaling at lower frequencies. The spectrum at point 2 shows a smaller range of frequencies with a −11/3 scaling, with a bump likely due
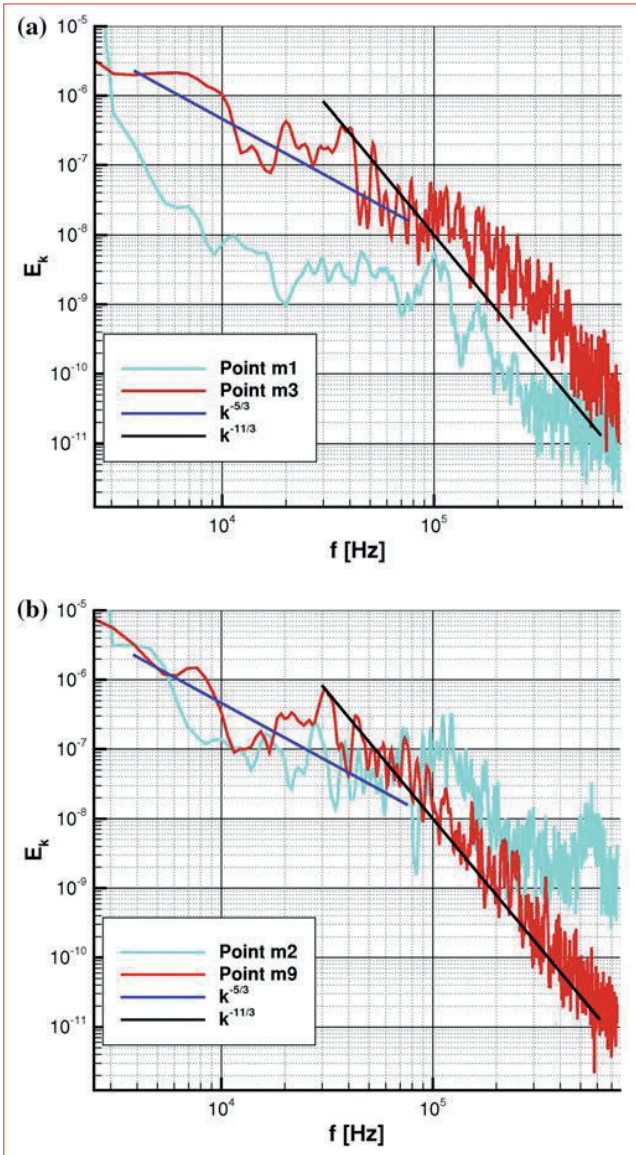
FIGURE 13 Turbulent kinetic energy spectra at some locations in the HyShot II scramjet engine, non-dimensionalized by their own variance and then normalized by the maximum amplitude among the four spectra

are larger, the mixing between fuel and oxidizer, occurring at molecular (dissipative) scales, can take place at larger ones. In other words, the turbulent kinetic energy cascade from integral to dissipative scales requires less scales to be completed. This conclusion has consequences also on reaction regime(s) and on combustion modelling. Indeed, in supersonic combustion, smaller Eddies may become larger than the flame thickness; if so, the smallest vortices can only wrinkle the flame without entering it. A second conclusion of importance to modellers is that any Computational Fluid Dynamic approach (CFD) must account for the above-stated findings when building an SGS model.

Conclusions

Numerical, experimental and theoretical results show the importance of understanding the physics of compressible flows and, in particular, mixing and combustion. In this paper, LES of the HyShot II test case confirms that air/hydrogen mixing (promoted by high streamwise and spanwise vorticity) and chemical kinetics are very fast, allowing complete combustion in the HyShot II ground tested combustor. The spectral analysis of turbulent kinetic energy has shown that the inertial range slope of turbulent kinetic energy versus wave number becomes steeper than that predicted by the Kolmogorov theory, beyond a certain high frequency. This steeper slope is in agreement with theoretical expectations and with experimental measurements in other test cases. Hence, dissipative scales are expected to be larger than in the subsonic regime. This conclusion is important both from a numerical and a physical point of view, justifying the quick mixing in supersonic flows and providing some guidelines on modelling turbulent scales in Large Eddy Simulation. From the numerical point of view, these results are very strong since they imply that, in order to capture, all the different scales of turbulence and, then, the major part of turbulent kinetic energy in a simulation, it is not necessary to have the same fine grid resolution as a subsonic flow, with a consequently saving of computational time.

Donato Cecere, Eugenio Giacomazzi,
Franca Rita Picchia, Nunzio M. Arcidiacono
ENEA, Sustainable Combustion Processes Laboratory

to the instability of the bow shock and to the strong expansion wave immediately after it.

Due to the need, in scramjet engines, to mix and burn in a very short distance, the conclusions on the steeper scaling and on the larger dissipative scales in supersonic flows are important. In fact, when dissipative scales

1. Townend, L.H.: Domain of the Scramjet. Journal of Propulsion and Power 17(6), 2317–2334 (2001)
2. Fry, R.S.: A Century of Ramjet Propulsion Technology Evolution. Journal of Propulsion and Power 20(1), 27–58 (2004)
3. Frost, M., Paull, A., Alesi, H.: HyShot T4Supersonic Combustion Experiments, Report for NAG- 1–2113 (2001), http://ntrs.nasa. gov/archive/nasa/casi.ntrs.nasa. gov/20000037781_2000047702.pdf
4. Hannemann, K., Karl, S., Schramm, J. M., Steelant J.: Methodology of a Combined Ground Based Testing and Numerical Modelling Analysis of Supersonic Combustion Flow Paths. Shock Waves, 20:353–366, doi: 10.1007/s00193-010-0269-8 (2010)
5. Laurence, S., Martinez Schramm, J., Karl, S., Hannemann, K.: An Experimental Investigation of Steady and Unsteady Combustion Phenomena in the HyShot II Combustor. AIAA Paper 2011–2310
6. Laurence, S., Martinez Schramm, J., Karl, S., Hannemann, K.: Ground-based Testing of the Hyshot II Combustor Using OH* Chemiluminescence. In Proceedings of the 7th European Symposium on Aerothermodynamics for Space Vehicles, Brugge, Belgium, 9–11 May (2011)
7. Won, S.H., Jeung, I.S., Choi, J.Y.: Turbulent Combustion Characteristics in HyShot Model Combustor with Transverse Fuel Injection. In Proceedings of the 43rd AIAA/ASME/SAE/ASEE Joint Propulsion Conference, AIAA paper 2007–5427
8. Poinsot, T.J., Lele, S.K.: Boundary Conditions for Direct Simulations of Compressible Viscous Flow. Journal of Computational Physics 101, 104–129 (1992)
9. Polifke, W., Wall, C.: Non-reflecting Boundary Conditions for Acoustic Transfer Matrix Estimation with LES, pp. 345–356. Proceedings of Summer Program, Center for Turbulence Research, Stanford, USA (2002)
10. Verzicco, R., Mohd-Yusof, J., Orlandi, P., Haworth, D.: Large Eddy Simulation in Complex Geometry Configurations Using Boundary Body Forces. AIAA J. 38, 427–433 (2000)
11. Verzicco, R., Iaccarino, G., Fatica, M., Orlandi, P.: Flow in an Impeller Stirred Tank Using an Immersed Boundary Method. Annual Research Briefs, NASA Ames Research Center/Stanford University Center for Turbulence Research. pp. 417–44 (2000)
12. Hirschfelder, J.O., Curtiss, C.F., Bird, R.B., Spotz, E.L.: The Molecular Theory of Gases and Liquids. John Wiley, New York (1954)
13. Bird, R.B., Stewart, W.E.: Lightfoot. Transport Phenomena, Wiley International Edition, E.N. (2002)
14. Wilke, C.R.: A Viscosity Equation for Gas Mixtures. J. Chem. Phys., 18:4:517–519, http://dx.doi.org/10.1063/1.1747673 (1950)
15. Kee, R.J., Dixon-Lewis, G., Warnatz, J., Coltrin, M.E., Miller, J.A., Moffat, H.K.: The CHEMKIN Collection III: Transport. Reaction Design (1998)
16. Mathur, S., Tondon, P.K., Saxena, S.C.: Thermal Conductivity of Binary, Ternary and Quaternary Mixtures of Rare Gases. Molecular Physics 12(6), 569–579 (1967)
17. Giacomazzi, E., Picchia, F.R., Arcidiacono, N.M.: A Review on Chemical Diffusion, Criticism and Limits of Simplified Meth-ods for Diffusion Coefficients Calculation. Combustion Theory and Modelling, 12:1, 135–158. http://dx.doi.org/10.1080/ 13647830701550370 (2008)
18. Giacomazzi, E., Bruno, C., Favini, B.: Fractal Modelling of Turbulent Mixing. Combustion Theory and Modelling 3, 637–655 (1999)
19. Giacomazzi, E., Bruno, C., Favini, B.: Fractal Modelling of Turbulent Combustion. Combustion Theory and Modelling 4, 391–412 (2000)
20. Giacomazzi, E., Battaglia, V., Bruno, C.: The Coupling of Turbulence and Chemistry in a Premixed Bluff-Body Flame as Studied by LES. Combustion and Flame 138, 320–325 (2004)
21. Sankaran, V., Porumbel, I., Menon, S.: Large Eddy Simulation of a Single-Cup Gasturbine Combustor Flows. In Proceedings of the 39th AIAA/ASME/SAE/ASEE Joint Propulsion Conference, AIAA paper 2003–5083
22. Génin, F., Menon, S.: Studies of Shock/turbulent Shear Layer Inter-action Using Large Eddy Simulation. Computers and Fluids 39, 800–819 (2010)
23. Magnussen, B.F.: The Eddy Dissipation Concept for Turbulent Combustion Modeling. Its Physical and Practical Implications. Norwegian Institute of Technology, Report N-7034, Trondheim, Norway, October 17 (1989)
24. Maas, U., Warnatz, J.: Ignition Processes in Hydrogen-Oxygen Mixtures. Combustion and Flame 74, 53–69 (1988)
25. Kim, S.D., Lee, B.J., Lee, H.J., Jeng, I., Choi, J.: Realization of Contact Resolving Approximate Riemann Solvers for Strong Shock and Expansioon Flows. International Journal for Numerical Methods in Fluids 62(10), 1107–1133 (2010)
26. Nelson, C., Menon, S.: Unsteady Simulations of Compressible Spa-tial Mixing Layers. In proceeding of the 36th AIAA Aerospace Sciences Meeting, AIAA paper 98–0786. http://dx.doi.org/10.2514/ 6.1998-786
27. Shu, C.W., Osher, S.: Efficient Implementation of Essentially Non-oscillatory Shock-capturing Schemes. J. Comput. Phys. 77, 439–471 (1988)
28. Lesieur, M.: Turbulence In Fluids, Springer (2008)
29. Cecere, D., Ingenito, A., Romagnosi, L., Bruno, C., Giacomazzi, E.: Shock/Boundary Layer/Heat Release Interaction in the HyShot II Scramjet Combustor. In Proceeding of 46th AIAA/ASME/SAE/ASEE Joint Propulsion Conference, AIAA paper 2010–7066
30. Cecere, D., Ingenito, A., Giacomazzi, E., Romagnosi, L., Bruno, C.: Hydrogen/air Supersonic Combustion for Future Hyper-sonic Vehicles. International Journal of Hydrogen Energy 36(18), 11969–11984 (2011)
31. Karl, S., Schramm, J.M., Laurence, S., Hannemann K.: CFD Analysis of Unstart Characteristics of the HyShot II Scramjet Configuration in the HEG Shock Tunnel. In Proceedings of the 17th AIAA International Space Planes and Hypersonic Systems and Technology Conference, AIAA paper 2011–2309
32. Ben-Yakar, A., Mungal, M.G., Hanson, R.K.: Time Evolution and Mixing Characteristics of Hydrogen and Ethylene Transverse Jets in Supersonic CrossFlow. Physics of Fluids 18(2), 26101–26116 (2006)
33. Ingenito, A., Bruno, C.: Physics and Regimes in Supersonic Combustion. AIAA Journal 48, 515–525 (2010)
34. Nishioka, M., Sakaue, S., Komada, K., Sakoshi, H., Furukawa, I.: Mixing Transition in Supersonic Streamwise Vortices. Fluid Mechanics and its Application 79, 249–258 (2006)
35. Dimotakis, P.E.: Turbulent Mixing. Annual Review of Fluid Mechanics. 37, 329–356 (2005)
36. Swithenbank, J., Chigier, N. A.: Vortex Mixing for Supersonic combustion. In Proceedings of the 21st International Symposium on Combustion, The Combustion Institute, 12:1:1153–1162 (1969)
37. Gerlinger, P., Stollb, P., Kindler, M., Schneider, F., Aigner, M.: Numerical Investigation of Mixing and Combustion Enhancement in Supersonic Combustors by Strut Induced Streamwise Vorticity. Aerospace Science and Technology 12, 159–168 (2008)
38. Doerner, S.E., Cutler, A.D.: Effects of Jet Swirl on Mixing of a Light Gas Jet in a Supersonic Airstream. NASA CR-1999-209842 (1999)
39. Marzouk, Y. M., Ghoniem, A. F.: Mechanism of Streamwise Vor-ticity Formation in Transverse Jets. In Proceedings of 40th AIAA Aerospace Sciences Meeting and Exhibit (2002), AIAA paper 2002–1063
40. Kida, S., Orszag, S.A.: Energy and Spectral Dynamics in Decaying Compressible Turbulence. Journal of Scientific Computing 7(1), 3–34 (1992)
41. Biagioni, L., D'Agostino, L.: Measurement of Energy Spectra in Weakly Compressible Turbulence. In Proceedings of 30th AIAA Fluid Dynamics Conference, Norfolk, VA (1999)
42. Kritsuk, A.G., Padoan, P., Wagner, R., Norman, M.L.: Scaling Laws and Intermittency in Highly Compressible Turbulence. AIP Conference Proceedings 932, 393–399 (2007)